# Complete Photoionization Experiments via Ultrafast Coherent Control with Polarization Multiplexing

P. Hockett*
*National Research Council of Canada, 100 Sussex Drive, Ottawa K1M 1R6, Canada*

M. Wollenhaupt
*Institut für Physik, Carl von Ossietzky Universität Oldenburg, Carl-von-Ossietzky-Straße 9-11, 26129 Oldenburg, Germany*

C. Lux and T. Baumert
*Institut für Physik, Universität Kassel, Heinrich-Plett-Straße 40, 34132 Kassel, Germany*
(Received 13 March 2014; published 5 June 2014)

Photoelectron angular distributions (PADs) obtained from ionization of potassium atoms using moderately intense femtosecond IR fields ($\sim 10^{12}$ W cm$^{-2}$) of various polarization states are shown to provide a route to "complete" photoionization experiments. Ionization occurs by a net three-photon absorption process, driven via the $4s \rightarrow 4p$ resonance at the one-photon level. A theoretical treatment incorporating the intrapulse electronic dynamics allows for a full set of ionization matrix elements to be extracted from 2D imaging data. 3D PADs generated from the extracted matrix elements are also compared to experimental, tomographically reconstructed, 3D photoelectron distributions, providing a sensitive test of their validity. Finally, application of the determined matrix elements to ionization via more complex, polarization-shaped, pulses is demonstrated, illustrating the utility of this methodology towards detailed understanding of complex ionization control schemes and suggesting the utility of such "multiplexed" intrapulse processes as powerful tools for measurement.

DOI: 10.1103/PhysRevLett.112.223001 PACS numbers: 32.80.Fb, 32.80.Qk, 32.80.Rm

So-called "complete" measurements of ionization dynamics aim to obtain the amplitudes and phases of the ionization matrix elements which describe the ionization event in terms of the partial wave decomposition of the outgoing photoelectron [1,2]. Since determining the phases requires an observable in which interferences between partial waves are present, photoelectron angular distributions (PADs) are required for complete measurements. Such experiments have long been performed for atomic systems [1,3] where, for example, PADs obtained via pump-probe schemes utilizing linearly polarized light and a range of pump-probe geometries [4–6], or different polarization states [7], have allowed the relative amplitude and phase of two ionization matrix elements to be determined [8]. For molecules, various experimental techniques, including molecular frame PADs [9–11], time-resolved rotational wave packet studies [12,13], and state-resolved measurements [14–16], have been demonstrated. The common thread to all of these measurements is the necessity of a data set containing sufficient information to reliably obtain the set of ionization matrix elements (which may be large) via some type of fitting procedure. Here "sufficient" refers to both the size of the experimental data set and the fundamental level of detail present [2]. For example, measurements from the Zare group demonstrated the level of detail obtainable via polarization [14,15]; work from Elliott's group investigated the role of interferences between one and two photon ionization pathways, including control of PADs [17–19].

Generalized control schemes utilizing shaped laser pulses can be considered as intrapulse pump-probe experiments; in this context, such schemes constitute highly multiplexed light-matter interactions, in which a large parameter space is interrogated coherently in the time domain, and could be considered as a natural continuation of serial measurement schemes for measuring atomic and molecular properties. Furthermore, measurement of the physical properties relevant to the control scheme allows the control processes to be understood in detail, rather than treated as a black-box optimization scheme, as pointed out in Refs. [20,21]. In this Letter, we demonstrate this principle using an experimental scheme originally designed with the aim of controlling PADs [22,23] but, instead, make use of the data to elucidate the ionization matrix elements. Because of the high information content of the PADs obtained, four experimental measurements prove sufficient for a determination of the ionization matrix elements in this case. The treatment presented herein can readily be extended to more complex, arbitrarily shaped pulses, and also to more complex ionization processes, including molecular ionization in cases where the intrapulse dynamics is computationally tractable, allowing for truly multiplexed measurements beyond the proof of concept shown here. We demonstrate this principle by application of the determined matrix elements to ionization via a polarization-multiplexed pulse.

 

The experimental setup has been covered in detail in Refs. [22,24,25]. Here, we briefly outline the control scheme for the case of polarization shaped pulses. Moderately intense ($\sim 10^{12}$ W cm$^{-2}$) laser pulses (795 nm, 30 fs, bandwidth 60 meV FWHM) were focussed into potassium vapor (generated by a dispenser source) in the interaction region of a velocity-map imaging spectrometer, allowing measurement of 2D projections of the full 3D photoelectron distribution. Basic control of the ellipticity of the pulse was achieved via a $\lambda/4$ plate, while more complex pulse shapes were attained with the use of a spatial light modulator in a $4f$ configuration [22,26]. In the case of cylindrically symmetric distributions, a single 2D projection is sufficient to reconstruct the full 3D distribution via standard inversion techniques [27]; for noncylindrically symmetric distributions, several projections must be obtained and a tomographic reconstruction technique applied to obtain the original 3D distribution [24,28,29].

In order to understand and treat the intrapulse light-matter interaction (i.e., simultaneous excitation and ionization dynamics) we split the problem conceptually into two steps, (1) a nonperturbative absorption at the one-photon level, the "pump" step, (2) a perturbative two-photon ionization, the "probe" step [30]. This is essentially an intrapulse $1+2$ resonance-enhanced multiphoton ionization scheme, where the first step is near resonant with the potassium $4s \rightarrow 4p$ transition, and the second step is nonresonant. A schematic of the ionization pathways for this net three-photon absorption process is given in Fig. 1.

The pump process describes the interaction of the control field with the atom at the one-photon level. With a moderately intense, near resonant field, coherent population transfer is driven. These Rabi oscillations follow the driving electric field and, crucially, depend sensitively on the instantaneous properties of the light field. The population dynamics during the laser pulse are then given by the time-dependent Schrödinger equation,

$$\frac{d}{dt}\begin{pmatrix} s(t) \\ p_{+1}(t) \\ p_{-1}(t) \end{pmatrix} = i\begin{pmatrix} 0 & \frac{1}{2}\Omega_L^*(t) & \frac{1}{2}\Omega_R^*(t) \\ \frac{1}{2}\Omega_L(t) & \delta_{+1} & 0 \\ \frac{1}{2}\Omega_R(t) & 0 & \delta_{-1} \end{pmatrix}\begin{pmatrix} s(t) \\ p_{+1}(t) \\ p_{-1}(t) \end{pmatrix}, \tag{1}$$

where $s(t)$, $p_{+1}(t)$, and $p_{-1}(t)$ are the state vector components for the $4s$ and $4p(m=\pm 1)$ states; $\Omega_{L/R}(t) = \mu_{L/R}E_{L/R}(t)$ are Rabi frequencies, where $\mu_{L/R}$ are the transition amplitudes, and $E_{L/R}(t)$ represents the electric field expanded in a spherical basis; $\delta_{\pm 1}$ represents the detuning of the laser from the resonant frequency of the transition. In this work, $\mu_{L/R}$, $E_0$ (total electric field strength) and $\hbar$ are all set to unity. For determination of PADs, these simplifications are acceptable as only the relative population of $m=\pm 1$ states will affect the angular distribution [31]. To define the polarization state of the light, a spectral phase $\phi_y$ is applied to the $y$ component of the $E$ field [22]. An example of the population dynamics is given in Fig. 1, illustrating how the difference in magnitudes of the $E_L(t)$ and $E_R(t)$ components describing an elliptically polarized field give rise to different $p_{+1}$ and $p_{-1}$ populations.

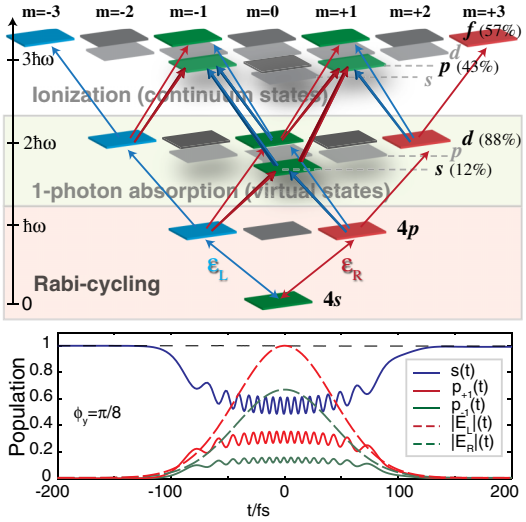


FIG. 1 (color online). Schematic of the three-photon ionization scheme for potassium. $|l,m\rangle$ states colored red or blue are accessed by $E_R$ or $E_L$ components of the field only, while states colored green can be accessed by both components via different pathways. Percentages are from Table I. The lower panel shows an example of the population dynamics and the envelope of the laser pulse.

The probe process describes the subsequent absorption of two photons resulting in ionization of the $4p$ excited state. Generally, the ionization matrix elements for a one-photon ionization process can be written as $\langle \psi_e; \psi_i | \boldsymbol{\mu}\cdot\mathbf{E} | \psi_n \rangle$, where the subscripts denote the free electron ($\psi_e$), ion ($\psi_i$), and neutral ($\psi_n$) wave functions, respectively, and $\boldsymbol{\mu}\cdot\mathbf{E}$ defines the light-matter coupling; this matrix element can be conveniently decomposed into radial and angular parts [32]. For the specific case at hand, the two-photon transition amplitude for a transition from state $|l_i, m_i\rangle$ to a final state $|l_f, m_f\rangle$, via a virtual intermediate state $|l_v, m_v\rangle$, can be written as a product of one-photon transitions integrated over the laser pulse

$$d_{l_f m_f}(k) = \int d_{i\rightarrow v}(k,t) d_{v\rightarrow f}(k,t)dt = \int dt \sum_{\substack{l_i,m_i;l_v,m_v \\ q,q'}} R_{l_v l_f}(k)\langle l_f m_f, 1q' | l_v m_v\rangle R_{l_i l_v}(k)\langle l_v m_v, 1q | l_i m_i\rangle E_{q'}(t)E_q(t)p_{m_i}(t), \tag{2}$$

where the summation is over all pathways from the initial, ionizable, states $|l_i, m_i\rangle$, weighted by their populations $p_{m_i}(t)$, and all polarization states $q$. Here, $R_{l_i l_f}(k)$ are the radial components and $\langle l_f m_f, 1q|l_i m_i\rangle$ are Clebsch-Gordan coefficients which describe the angular momentum coupling. In writing this form, we have assumed that (a) the dipole approximation applies [32], (b) that the ionization can be treated perturbatively, hence, the resultant matrix elements are independent of the instantaneous pulse intensity (i.e., constant over the pulse envelope), and (c) a single active electron picture with no angular momentum coupling of the virtual and final one-electron states to the nascent ion core. We note that, most generally, these approximations could be removed, resulting in a more complex angular momentum coupling scheme with additional partial wave components due to additional electron-ion scattering, and intensity-dependent $R_{l_i l_f}(k)$.

The observed photoelectron yield as a function of angle, for a single $k$ or small energy range $dk$ over which we assume the $R(k)$ can be regarded as constant, is then given by the coherent square over all final (photoelectron) states

$$I(\theta,\phi;k) = \sum_{\substack{l_f, m_f \\ l'_f, m'_f}} d_{l_f m_f}(k) Y_{l_f m_f}(\theta,\phi) d^*_{l'_f m'_f}(k) Y^*_{l'_f m'_f}(\theta,\phi), \tag{3}$$

where the $Y_{lm}(\theta,\phi)$ are spherical harmonics.

Finally, we note that the PAD can also be described phenomenologically by $\beta_{LM}$ parameters [1], where

$$I(\theta,\phi;k) = \sum_{L,M} \beta_{LM}(k) Y_{LM}(\theta,\phi). \tag{4}$$

The information content of the observed PADs can be considered in terms of the number of $L$, $M$ terms present in this expansion, which will, therefore, depend on both the inherent properties of the system and the laser pulse parameters, as shown in Eq. (2). For example, use of linearly polarized light restricts Eq. (4) to terms with $M = 0$ only.

In order to apply the preceding treatment, the angular momentum coupling coefficients are calculated analytically and the population dynamics numerically, leaving only the $R_{ll}$ as unknowns: determination of these complex radial matrix elements is the aim of "complete" photoionization experiments. To generate 3D photoelectron distributions, PADs calculated according to Eq. (3) were convoluted with a Gaussian radial distribution; 2D image-plane projections were generated by summation of the 3D gridded volumetric data. Although numerically intensive, this procedure generates 2D projections that can be compared directly with 2D experimental imaging data even in the case of non-cylindrically symmetric distributions. The $R_{ll}$ were then determined by optimizing the computed 2D projections. In this procedure, the $R_{ll}$ were expressed in magnitude and phase form, $R_{ll} = |R_{ll}|e^{i\delta_{ll}}$, where $-\pi \le \delta_{ll} \le \pi$; also, $R_{l_1 l_2} = R^*_{l_2 l_1}$. Because absolute phases cannot be determined, $\delta_{01}$ at the one-photon level was set to zero as a reference phase. Technical details of this fitting procedure, including uncertainty estimates and Monte Carlo sampling of the fitting parameter ($\chi^2$) hyperspace, will be given in a future publication [33].

The best fit images are shown in Figs. 2(a)–2(d). The fitted results show a reasonable agreement with the experimental data in terms of the form of the angular distributions, and trend with polarization but a less satisfactory agreement in terms of the width and scaling of the features; we attribute this to the assumption of a Gaussian radial distribution. Nonetheless, the obtained ionization matrix elements appear to be relatively insensitive to these issues because they are primarily defined by the angular coordinate of the image. The calculated $\beta_{LM}$, as a function of $\phi_y$, are shown in Fig. 2(e). Nonzero values are found for $L = 0, 2, 4, 6$ and even $M$ terms, consistent with the

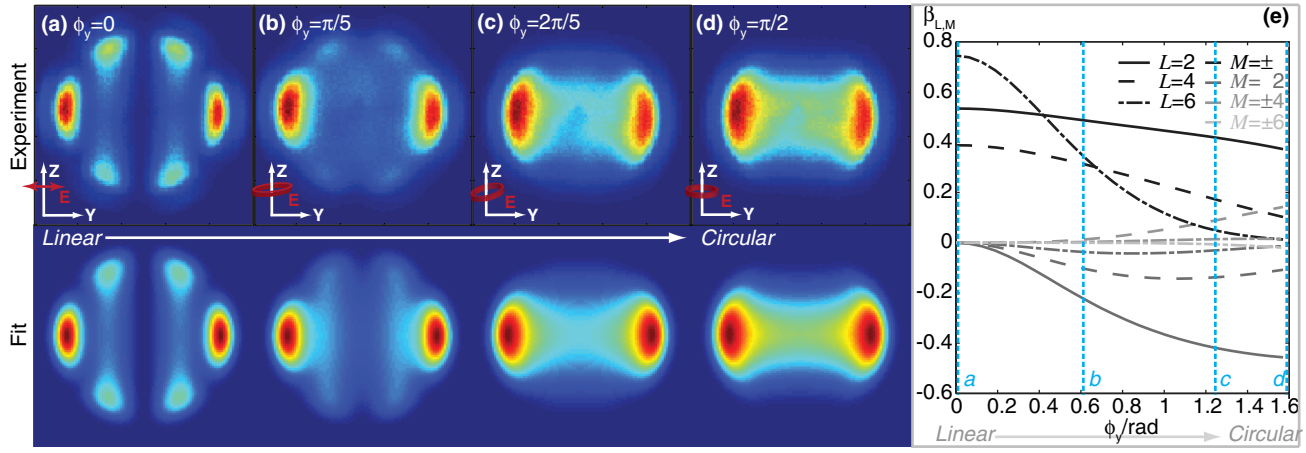


FIG. 2 (color online). Experimental and computed 2D photoelectron velocity map images. (a)–(d) Raw experimental data and fit results. The laser propagates along the $z$ axis; electrons are detected or integrated in the $(y, z)$ plane. (e) Calculated $\beta_{LM}$ parameters [Eq. (4)] as a function of polarization ($\phi_y$)

TABLE I. Fitted values for the relative transition matrix element magnitudes, $|R_{ll}|$, and phases, $\delta_{ll}$. The square of the magnitudes is expressed as a percentage of the total transition amplitude, normalized to unity for each step (these percentages are also shown in Fig. 1). Uncertainties in the last digit are given in parentheses.

| Transition | | | $\lvert R_{l_1 l_2}\rvert$ | $\lvert R_{l_1 l_2}\rvert^2$/% | $\delta_{l_1 l_2}$/rad. |
|---|---|---|---|---|---|
| $l_1$ | $l_2$ | | | | |
| $i \to v$ | p | s | 0.34 (3) | 12 (4) | 0[a] |
| | p | d | 0.94 (8) | 88 (11) | −1.62(4) |
| $v \to f$ | s | p | 0.85 (8) | 72 (12) | −0.19(3) |
| | d | p | 0.14 (2) | 2 (2) | −2.08(8) |
| | d | f | 0.51 (9) | 26 (13) | 0.24 (7) |

[a]Reference phase, set to zero during fitting.

experimental symmetry and the total number of photons absorbed [1], and a smooth variation in the parameters is observed with ellipticity.

The fitted parameters obtained are given in Table I. Here, the magnitudes are normalized to give total cross sections of unity at the one-photon and two-photon levels. The results show that the final photoelectron wave function, summed over all paths to each final state $|R_{l_i l_f}|^2 = (\sum_v |R_{l_i l_v}||R_{l_v l_f}|)^2$, is 57% $f$ wave and 43% $p$ wave in character. This is consistent with the expectation from the shape of the PAD, which has strong $L = 6$ character, that the $f$ wave dominates, but also reveals a significant contribution from $l = 1$ partial waves, primarily via the $p \to s \to p$ channel. The relative phases of the final continuum waves are quite different, revealing partially destructive interference between the $p$ and $f$ waves. It is interesting to note that since the scattering phase and Wigner delay are directly related [34], these phase differences indicate a significant difference in emission time of all the continuum waves, including a dependence on the virtual state since the $p \to s \to p$ and $p \to d \to p$ paths accumulate different total phases [35].

To further validate these results, we next consider in detail the full 3D distributions. Figure 3 shows the 3D photoelectron distributions for two polarization states. The experimental data [Figs. 3(a) and 3(c)] were tomographically reconstructed from a set of 2D images, as detailed in Ref. [24]. The tomographic data provides a full 3D map of the PADs, providing details which may be obscured in single 2D projections of noncylindrically symmetric distributions. This data compares well to the calculated distributions, Figs. 3(b) and 3(d), with $R_{ll}$ based only on fitting of the less detailed 2D projections, confirming that the full angular structure is well determined by the fitted matrix elements. The fit results were further validated at the level of the $\beta_{LM}$ parameters [Eq. (4)]; this analysis will be discussed in a future publication [33].

Finally, we illustrate, in Fig. 4, the application of the ionization matrix elements determined above to the case of more complex polarization-shaped pulses. For such polarization-shaped pulses, the PAD can be considered as a coherent sum over the "basis states" given by the PADs correlated with individual polarization states, as defined by the $\beta_{LM}(\phi_y)$ expansion in Fig. 2(e); an experiment utilizing a polarization-shaped pulse, thus, constitutes a highly multiplexed interrogation of the light-matter interaction in polarization space. Consequently, the PAD may be highly structured, and is extremely sensitive to the exact shape of the laser pulse, which affects the contributions of each ionization pathway to the coherent summation (see Supplemental Material [36]).

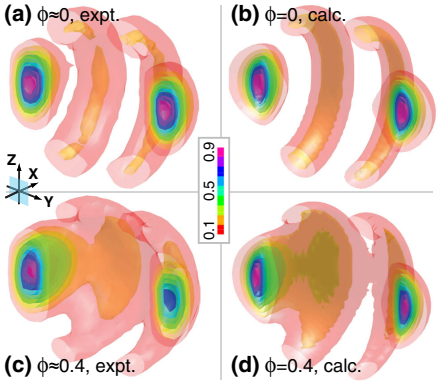


FIG. 3 (color online). Experimental and computed 3D photoelectron velocity distributions. (a),(c) Measured distributions obtained via tomographic reconstruction; (b),(d) calculated distributions based on the fitted ionization matrix elements.

In this work, we have demonstrated the utility of complex intrapulse light-matter interactions as a means to complete photoionization experiments. This methodology is applicable to any arbitrarily shaped laser field, providing the ionization can be treated perturbatively and the photoelectron energy spread is small [with respect to the response of $R(k)$], thus, enabling a route to designing control fields with full understanding of the control process. Combined with tomographic reconstruction, or other means of obtaining full 3D PADs, this should be a powerful technique for understanding the

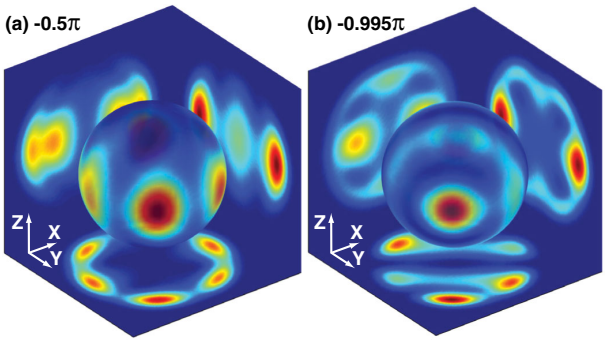


FIG. 4 (color online). Calculated 3D PADs and 2D projections for $E_{X,Y}(t)$ obtained by application of a spectral phase mask to the red half of the spectrum (similar to the experimental pulses discussed in Ref. [22]) of (a) $\phi_y = -\pi/2$ and (b) $\phi_y = -0.995\pi$.

ionization dynamics in many atomic systems and should be extensible to the more complex case of molecular ionization dynamics, including multiphoton ionization of chiral molecules (which exhibits photoelectron circular dichroism [37,38]), with the inclusion of the relevant angular momentum couplings in Eq. (2) [39]. With the ongoing interest in PADs in many related contexts [40]—most generally as probes of molecular dynamics—our methodology has great potential for detailed understanding of the role of ionization in a range of measurements. The extraction of the ionization matrix elements from experimental data in general wave packet dynamics experiments would represent a significant step beyond the semiquantitative models applied so far [41], although such problems will naturally be challenging. Finally, we note the possibility of turning the methodology around, and using well-characterized processes with known ionization dynamics as *in situ* probes of complex laser fields in a manner analogous to other ionization-based methods used for attosecond pulse metrology [42].

We thank Albert Stolow for suggesting this collaboration. We thank one of the referees of this Letter for suggesting the application to pulse metrology.

*paul.hockett@nrc.ca

[1] K. L. Reid, Annu. Rev. Phys. Chem. **54**, 397 (2003).
[2] N. Cherepkov, J. Electron Spectrosc. Relat. Phenom. **144–147**, 1197 (2005).
[3] U. Becker, J. Electron Spectrosc. Relat. Phenom. **96**, 105 (1998).
[4] J. A. Duncanson, M. P. Strand, A. Lindgård, and R. S. Berry, Phys. Rev. Lett. **37**, 987 (1976).
[5] J. C. Hansen, J. A. Duncanson, R.-L. Chien, and R. S. Berry, Phys. Rev. A **21**, 222 (1980).
[6] R.-L. Chien, O. C. Mullins, and R. S. Berry, Phys. Rev. A **28**, 2078 (1983).
[7] H. T. Duong, J. Pinard, and J. L. Vialle, J. Phys. B **11**, 797 (1978).
[8] P. Lambropoulos, J. Phys. B **6**, L319 (1973).
[9] O. Geßner, Y. Hikosaka, B. Zimmermann, A. Hempelmann, R. R. Lucchese, J. H. D. Eland, P.-M. Guyon, and U. Becker, Phys. Rev. Lett. **88**, 193002 (2002).
[10] M. Lebech, J. C. Houver, A. Lafosse, D. Dowek, C. Alcaraz, L. Nahon, and R. R. Lucchese, J. Chem. Phys. **118**, 9653 (2003).
[11] A. Yagishita, K. Hosaka, and J.-I. Adachi, J. Electron Spectrosc. Relat. Phenom. **142**, 295 (2005).
[12] T. Suzuki, Annu. Rev. Phys. Chem. **57**, 555 (2006).
[13] Y.-I. Suzuki, Y. Tang, and T. Suzuki, Phys. Chem. Chem. Phys. **14**, 7309 (2012).
[14] D. J. Leahy, K. L. Reid, and R. N. Zare, J. Chem. Phys. **95**, 1757 (1991).
[15] K. L. Reid, D. J. Leahy, and R. N. Zare, Phys. Rev. Lett. **68**, 3527 (1992).
[16] P. Hockett, M. Staniforth, K. L. Reid, and D. Townsend, Phys. Rev. Lett. **102**, 253002 (2009).
[17] Y.-Y. Yin, C. Chen, D. S. Elliott, and A. V. Smith, Phys. Rev. Lett. **69**, 2353 (1992).
[18] Y.-Y. Yin, D. S. Elliott, R. Shehadeh, and E. R. Grant, Chem. Phys. Lett. **241**, 591 (1995).
[19] Z.-M. Wang and D. S. Elliott, Phys. Rev. Lett. **87**, 173001 (2001).
[20] M. Wollenhaupt, A. Präkelt, C. Sarpe-Tudoran, D. Liese, and T. Baumert, J. Opt. B **7**, S270 (2005).
[21] M. Wollenhaupt and T. Baumert, Faraday Discuss. **153**, 9 (2011).
[22] M. Wollenhaupt, M. Krug, J. Köhler, T. Bayer, C. Sarpe-Tudoran, and T. Baumert, Appl. Phys. B **95**, 245 (2009).
[23] M. Wollenhaupt, C. Lux, M. Krug, and T. Baumert, ChemPhysChem **14**, 1341 (2013).
[24] M. Wollenhaupt, M. Krug, J. Köhler, T. Bayer, C. Sarpe-Tudoran, and T. Baumert, Appl. Phys. B **95**, 647 (2009).
[25] M. Krug, T. Bayer, M. Wollenhaupt, C. Sarpe-Tudoran, T. Baumert, S. S. Ivanov, and N. V. Vitanov, New J. Phys. **11**, 105051 (2009).
[26] A. Präkelt, M. Wollenhaupt, A. Assion, C. Horn, C. Sarpe-Tudoran, M. Winter, and T. Baumert, Rev. Sci. Instrum. **74**, 4950 (2003).
[27] *Imaging in Molecular Dynamics: Technology and Applications*, edited by B. J. Whitaker (Cambridge University Press, Cambridge, England, 2003).
[28] C. Smeenk, L. Arissian, A. Staudte, D. M. Villeneuve, and P. B. Corkum, J. Phys. B **42**, 185402 (2009).
[29] P. Hockett, M. Staniforth, and K. L. Reid, Mol. Phys. **108**, 1045 (2010).
[30] M. Wollenhaupt, A. Assion, O. Bazhan, C. Horn, D. Liese, C. Sarpe-Tudoran, M. Winter, and T. Baumert, Phys. Rev. A **68**, 015401 (2003).
[31] For the same reason, the value of $\delta_{\pm 1}$ has no effect on the PADs in this case, except as a scaling factor for the total population transfer at the one-photon level; in the calculations shown in Fig. 1 $\delta_{\pm 1} = 0.05$ rad/fs. For completeness, we also note that spin is neglected in this treatment.
[32] J. Cooper and R. N. Zare, in *Lectures in Theoretical Physics: Atomic Collision Processes*, edited by S. Geltman, K. T. Mahanthappa, and W. E. Brittin (Gordon and Breach, New York, 1969), Vol. XI-C, pp. 317–337.
[33] P. Hockett, C. Lux, M. Wollenhaupt, and T. Baumert (to be published).
[34] E. P. Wigner, Phys. Rev. **98**, 145 (1955).
[35] We note, for completeness, that, because the Wigner delay is the energy derivative of the scattering phase, it is not defined in absolute terms by the relative phases at a single energy, but relative emission times may be determined from a set of such results.
[36] See Supplemental Material at http://link.aps.org/supplemental/10.1103/PhysRevLett.112.223001 for extended discussion of PADs obtained via pulse shaping, with four pulses illustrated.
[37] C. Lux, M. Wollenhaupt, T. Bolze, Q. Liang, J. Köhler, C. Sarpe, and T. Baumert, Angew. Chem., Int. Ed. Engl. **51**, 5001 (2012).
[38] M. H. M. Janssen and I. Powis, Phys. Chem. Chem. Phys. **16**, 856 (2014).
[39] P. Hockett and K. L. Reid, J. Chem. Phys. **127**, 154308 (2007).
[40] K. L. Reid, Mol. Phys. **110**, 131 (2012).
[41] P. Hockett, C. Z. Bisgaard, O. J. Clarkin, and A. Stolow, Nat. Phys. **7**, 612 (2011).
[42] F. Krausz and M. Ivanov, Rev. Mod. Phys. **81**, 163 (2009).